Food and Chemical Toxicology 128 (2019) 256–266

Contents lists available at ScienceDirect

Food and Chemical Toxicology

journal homepage: www.elsevier.com/locate/foodchemtox

Decreased levels of H3K9ac and H3K27ac in the promotor region of ovarian P450 aromatase mediated low estradiol synthesis in female offspring rats induced by prenatal nicotine exposure as well as in human granulosa cells after nicotine treatment

Guanlan Fan[a,b,1], Qi Zhang[a,1], Yang Wan[a], Feng Lv[a], Yunxi Chen[a], Yuan Ni[a], Wen Zou[a], Wei Zhang[b], Hui Wang[a,b,c,*]

[a] Department of Pharmacology, Basic Medical School of Wuhan University, Wuhan, 430071, China
[b] Department of Obstetrics and Gynecology, Zhongnan Hospital of Wuhan University, Wuhan, 430071, China
[c] Hubei Provincial Key Laboratory of Developmentally Originated Disease, Wuhan, 430071, China

ARTICLE INFO

Keywords:
Nicotine
Ovarian development
Estradiol synthesis
Cytochrome P450 aromatase
Histone acetylation

ABSTRACT

Prenatal nicotine exposure (PNE) could induce ovarian dysplasia in offspring. This study aimed to confirm its intrauterine origin and explore a programming mechanism of ovarian dysplasia caused by PNE. Pregnant Wistar rats were injected subcutaneously with nicotine (2 mg/kg.d) from gestation day (GD) 9 to GD20. Serum of female offspring was obtained for hormone assays and ovarian tissues were collected. The results showed that PNE impaired ovarian development, and inhibited estradiol production and cytochrome P450 aromatase (P450arom) expression before and after birth. Moreover, the nicotinic acetylcholine receptors (nAChRs) expression was increased in utero, while histone 3 lysine 9 acetylation (H3K9ac) and H3K27ac levels in the P450arom promoter region were decreased persistently in PNE group before and after birth. In vitro, nicotine decreased P450arom expression and estradiol production in human granulosa cell line KGN. Furthermore, nicotine treatment up-regulated nAChRα6 and α9 expression and down-regulated the H3K9ac and H3K27ac levels of the P450arom promoter region. Non-specific nAChRs inhibitor vecuronium bromide reversed these effects. These results suggest that PNE could induce ovarian dysplasia and inhibit estradiol synthesis in the female offspring rats, which was related to the decreased H3K9ac and H3K27ac levels in the promotor region of the P450arom via the nAChRs.

1. Introduction

It has been well established that approximately 20%–50% of women smoked during pregnancy, and even 50% of pregnant women were exposed passively to cigarette smoking (Higgins, 2002; Contal et al., 2005). The exposure to smoking during pregnancy is associated with a number of adverse obstetrical outcomes, including placental damage, low birth weight of the fetus, and high risk of chronic diseases in adulthood (Bainbridge and Smith, 2006; Chen et al., 2007; Lim and Sobey, 2011). At the same time, a follow-up study of more than 20 years suggested that cigarette smoking exposure during pregnancy had adverse effects on the reproductive function of female offspring, such as the delayed age of menarche (Ernst et al., 2012). Cigarette smoke is a complex mixture of toxic chemicals, including nicotine, carbon monoxide, and several recognized carcinogens and mutagens, of which nicotine was considered to be one of the teratogenic factors that interfered with embryonic development (Yildiz, 2004). Animal studies have confirmed that prenatal nicotine exposure (PNE) disrupted ovarian function in adult female offspring rats, such as the weakened fertility and reduced serum estradiol level (Holloway et al., 2006). However, the underlying mechanism of ovarian developmental toxicity and estrogen synthesis inhibition caused by PNE still remains unclear.

Estradiol is known as the main active estrogen in ovarian steroid hormones and plays a pivotal role in female reproduction. Abnormal estradiol levels are related to many gynaecological diseases, such as polycystic ovary syndrome (PCOS) (Liu et al., 2017; Gupta et al., 2013). In addition, the estradiol level could also affect the function of other tissues (e.g. brain, bone, and heart) (Meitzen et al., 2018; Lang-

* Corresponding author. Department of Obstetrics and Gynecology, Zhongnan Hospital of Wuhan University, Wuhan, 430071, Hubei Province, China.
E-mail address: wanghui19@whu.edu.cn (H. Wang).
[1] Guanlan Fan and Qi Zhang contributed equally to this study.

https://doi.org/10.1016/j.fct.2019.03.055
Received 14 January 2019; Received in revised form 18 March 2019; Accepted 30 March 2019
Available online 06 April 2019
0278-6915/

Table 1
Oligonucleotide primers and PCR conditions in real-time quantitative PCR.

Genes	Forward primer	Reverse primer	Annealing
nAChRα7 (Rat)	GCACAATACTTCGCCAGCAC	TTCTGGTCCACTTAGGCATTTT	59 °C, 30 s
nAChRα9 (Rat)	CCTCGCTCCGTTGAGTTTCTA	GCAGTGATCAAGGCCATGGT	60 °C, 30 s
nAChRα10 (Rat)	GTCTGCCTTCCCTTTTGACG	AGCAGCAGCCATAGGTGAGG	60 °C, 30 s
nAChRβ1 (Rat)	AGAGACCAACTACCCGAACCAC	GCGTAGCTCCTGAGGCAGAC	60 °C, 30 s
nAChRβ3 (Rat)	GGAGATACTCAACGCAAAGGG	CTTCGTCCGAGGGTAGGTAGA	60 °C, 30 s
nAchRβ4 (Rat)	AGCCCATCCAACCTCTAT	GAAGCTGACACCCTCTAATG	60 °C, 30 s
StAR (Rat)	GGGAGATGCCTGAGCAAAGC	GCTGGCGAACTCTATCTGGGT	63 °C, 30 s
P450scc (Rat)	GCTGCCTGGGATGTGATTTTC	GATGTTGGCCTGGATGTTCTTG	63 °C, 30 s
3β-HSD (Rat)	TCTACTGCAGCACAGTTGAC	ATACCCTTATTTTTGAGGGC	58 °C, 30 s
17β-HSD1 (Rat)	CGTGGTTATGAGCAAGCCCT	AAGCGGTTTGTGGAGAAGTAGC	60 °C, 30 s
P450arom (Rat)	ATGGGCCTCCTTCTCCTGAT	CAGGCACTTCCAATCCCCAT	60 °C, 30 s
GAPDH (Rat)	GCAAGTTCAATGGCACAG	GCCAGTAGACTCCACGACA	60 °C, 30 s
nAChRα4 (Human)	CTCACCGTCCTTCTGTGTC	CTGGCTTTCTCAGCTTCCAG	63 °C, 30 s
nAChRα6 (Human)	TCCATCGTGGTGACTGTGT	AGGCCACCTCATCAGCAG	63 °C, 30 s
nAchRα9 (Human)	GAAAGCAGCCAGGAACAAAG	GCACTTGGCGATGTACTCAA	60 °C, 30 s
StAR (Human)	CCACTTGCATGGTGCTTCAC	GACCTGGTTGATGATGCTCTTG	60 °C, 30 s
P450scc (Human)	TCCGTCTGTTCAGGACCAAG	GTGCCATCTCATACAAGTGCC	60 °C, 30 s
3β-HSD (Human)	GCCTTCGGACCAGAATTGAG	ACATCAATGATACAGGCGGTGT	60 °C, 30 s
17β-HSD1 (Human)	GTGTATGCCACGTTGAGGGA	TCCGCACAGTCCCTACTACATT	60 °C, 30 s
P450arom (Human)	CAGCCTGTCGTGGACTTGGT	GGCGATGTACTTTCCTGCACA	58 °C, 30 s
GAPDH (Human)	CATCATCCCTGCCTCTACTGG	GTGGGTGTCGCTGTTGAAGTC	60 °C, 30 s

Muritano et al., 2018; Yang et al., 2018). Ovarian development and estradiol production of different species have their own time window, but most mammals have steroidogenic factor expression and estrogen synthesis ability since mid-pregnancy, which can be affected by some xenobiotics (Hogg et al., 2011; Knapczyk-Stwora et al., 2013; Tehrani et al., 2014). The granulosa cell is a functional cell that synthesizes estradiol, and in which the cytochrome P450 aromatase (P450arom) catalyzed the final rate limiting step in estradiol biosynthesis (Conley and Hinshelwood, 2001). A growing body of evidences have suggested that low expression of P450arom induced by adverse environmental conditions during pregnancy was an important cause for estrogen synthesis inhibition (Mahalingam et al., 2017). For example, after maternal exposure to bisphenol A during pregnancy, the P450arom expression and estrogen level in female offspring mice continuously decreased (Mahalingam et al., 2017); fructose intake during pregnancy also inhibited ovarian estradiol synthesis in rats, which was due to low P450arom expression (Munetsuna et al., 2018). However, it is unclear whether the PNE-induced estrogen synthesis inhibition of female offspring is associated with low P450arom expression in the ovary.

The epigenetic modifications were established during early development and may result in life-long programming (Jaenisch and Bird, 2003). An earlier study has shown that aberrant epigenetic modifications regulated the expression of genes involved in steroid hormone biosynthesis and action (Martinez-Arguelles and Papadopoulos, 2010). Recent reports from Mehta lab showed that histone H3 acetylation at Lys 9/14 (H3K9/14) was important for P450arom expression and estradiol production in buffalo granulosa cells during follicular development (Mehta et al., 2015). Apart from this, an analysis of histone modifications using ChIP assay revealed that chromatin remodeling through histone modifications were the regulatory mechanism controlling P450arom tissue-specific expression and promoter activity during folliculogenesis and luteinization (Monga et al., 2011). Therefore, we hypothesized that PNE disturbed histone modifications of P450arom, which might lead to ovarian dysplasia and estrogen synthetic inhibition throughout the life.

In the present study, we observed changes of ovarian morphology and estradiol synthetic function in female offspring by using a rat model as previously described (Xu et al., 2013). Furthermore, combination in vivo and in vitro experiments, we elucidated the intrauterine programming mechanism of ovarian estradiol synthetic inhibition by nicotine. This study provides experimental and theoretical evidences for the early prevention and treatment of PNE-induced ovarian related diseases.

2. Materials and methods

2.1. Drugs and reagents

Nicotine (N3876-25 ML) was purchased from Sigma-Aldrich Co., Ltd. (St. Louis, MO, USA). Vecuronium bromide (ab120536, Abcam) was obtained from Abcam (Cambridge, UK). Isoflurane was purchased from Baxter Healthcare Co. (Deerfield, IL, USA). Rat estradiol and testosterone enzyme-linked immunosorbent assay (ELISA) was obtained from R&D (Minneapolis, MN, USA). Rat/mouse iodine (125I) radioimmunoassay (RIA) kits of estradiol and testosterone were purchased from Beijing North Institute of Biological Technology (Beijing, China). TRIZOL was purchased from Invitrogen Co. (Carlsbad, CA, USA). Reverse transcription and real-time quantitative polymerase chain reaction (RT-qPCR) kits were purchased from Takara Biotech Co., Ltd. (Dalian, China). The SYBR Green dye was purchased from Applied Biosystems through Thermo Fisher scientific (ABI) (Foster City, CA, USA). All of the primers were synthesized by Tianyihuiyuan Biotech Co., Ltd. (Wuhan, China). The antibodies of Ki67 (ab16667) and P450arom (ab18995) were purchased from Abcam plc (Cambridge, Cambridge shire, UK). The antibody of cleaved Caspase-3 (RLT0656) was purchased from Ruiying Biotech Co. (Suzhou, China). The antibodies of anti-acetyl histone 3 lysine 9 (H3K9) (A7255), H3K27 (A7253), and goat anti-rabbit immunoglobulin G (IgG; AC005) were purchased from ABclonal Biotech Co., Ltd (Wuhan, China). The DNA purification kit (Q5314) was purchased from TIANGEN Biotech Co., Ltd. (Beijing, China). Other chemicals and reagents were of analytical grade.

2.2. Animals and treatment

Specific pathogen-free Wistar rats [No. 2012–2014, Certification No. 42000600002258, License No. SCXK (Hubei)] with weights of 209 ± 12 g (females) and 258 ± 17 g (males) were obtained from the Experimental Center of the Hubei Medical Scientific Academy (Wuhan, China). Animal experiments were performed in the Center for Animal Experiments of Wuhan University (Wuhan, China), which is accredited by the Association for Assessment and Accreditation of Laboratory Animal Care International (AAALAC International). The Committee on the Ethics of Animal Experiments of the Wuhan University School of

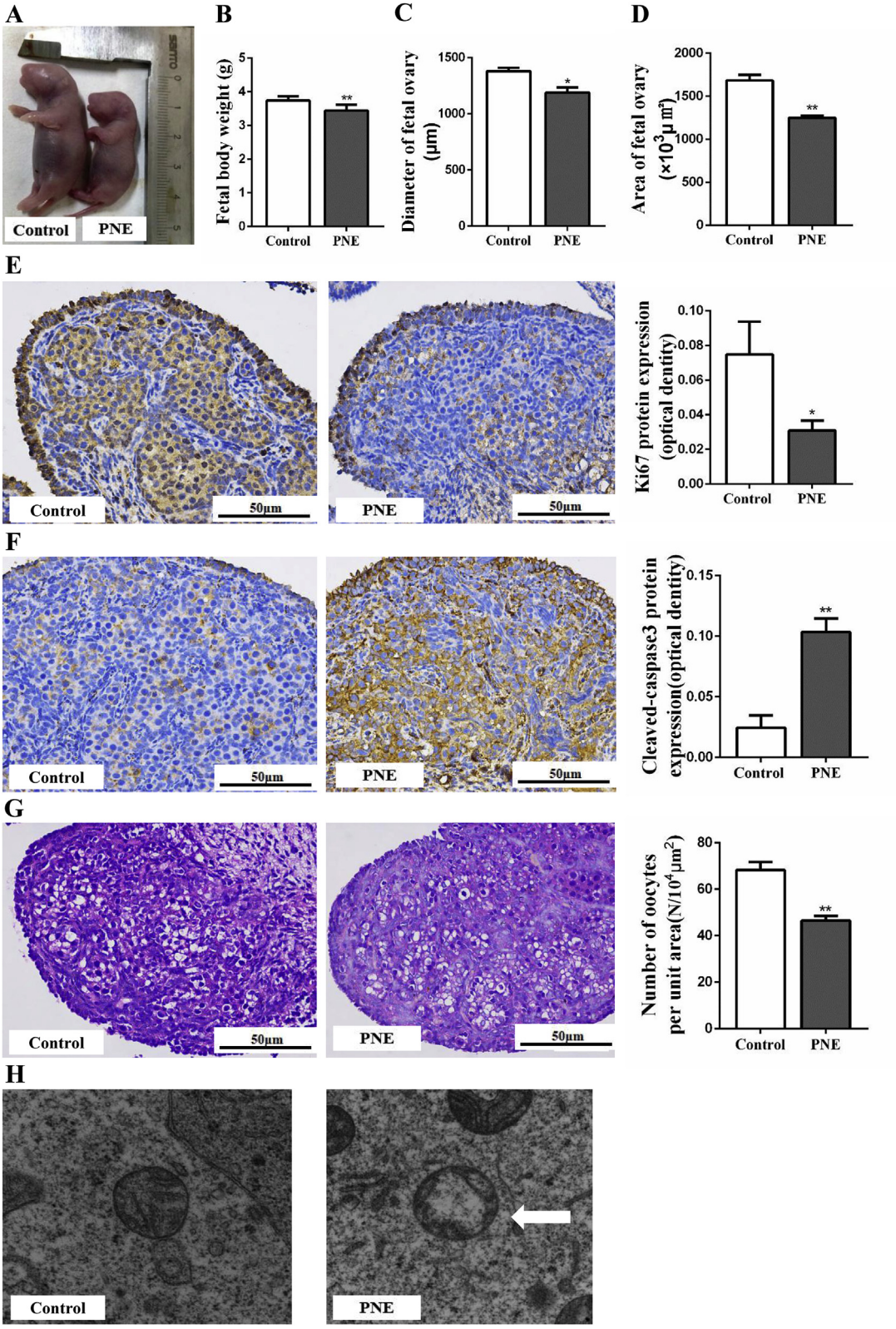

Fig. 1. Effects of prenatal nicotine exposure (PNE) on body weight and ovarian morphology in female fetal rats. A: picture of the fetus; B: fetal body weight (n = 12); C: diameter of fetal ovary (n = 5); D: area of fetal ovary (n = 5); E, F: Ki67 and cleaved caspase-3 protein expression (immunohistochemical, × 400), five sections of each group were selected and five random fields of each section were scored; G: the density of oocytes per unit area (10,000 μm^2), HE sections of each group were selected and calculated (n = 5); H: ultra-structure of ovarian pre-granulosa cells (white arrows: mitochondrion, transmission electron microscope, × 15000). Mean ± S.E.M., $^*P < 0.05$, $^{**}P < 0.01$ vs. control.

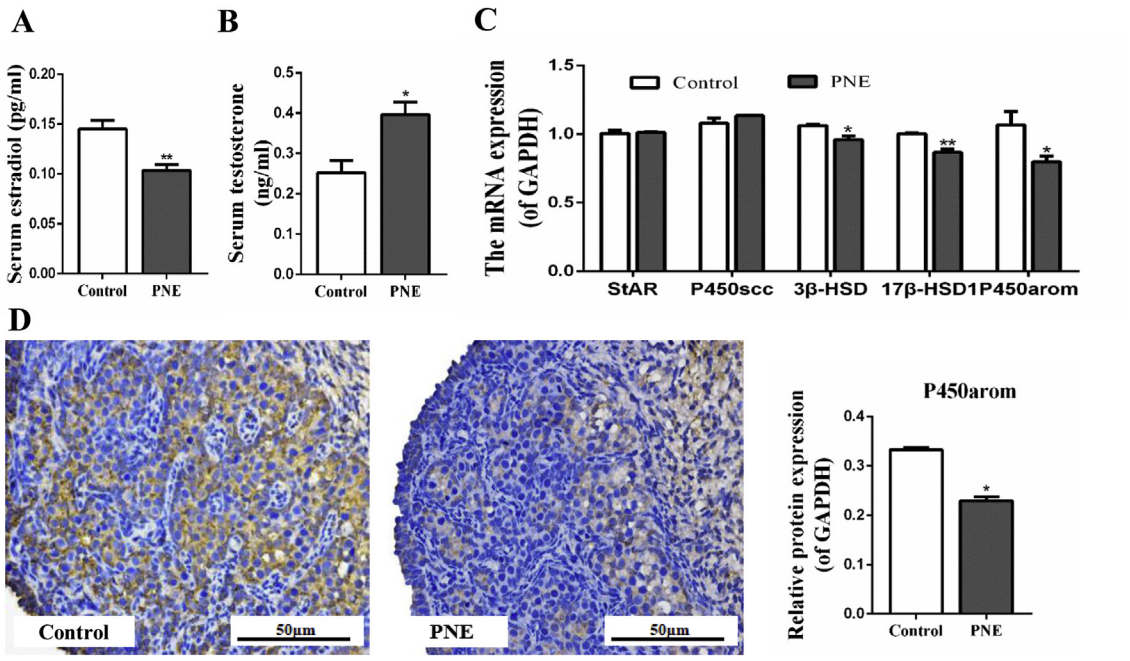

Fig. 2. Effects of prenatal nicotine exposure (PNE) on serum estradiol concentration and ovarian steroidogenic enzymes expression in fetal rats. A: fetal serum estradiol concentration (n = 4, blood from 3 to 4 littermates were pooled into one sample); B: fetal serum testosterone concentration (n = 4, blood from 3 to 4 littermates were pooled into one sample); C: the mRNA expression of StAR, P450scc, 3β-HSD, 17β-HSD1, and P450arom (n = 6, six pairs of fetal ovaries from two littermates were pooled for homogenization into one sample); D: P450arom protein expression (immunohistochemical, × 400) and mean optical density of P450arom protein expression, five sections of each group were selected and five random fields of each section were scored. Mean ± S.E.M., $^{*}P < 0.05$, $^{**}P < 0.01$ vs. control. GAPDH, glyceraldehyde phosphate dehydrogenase; StAR, steroidogenic acute regulatory protein; P450scc, cytochrome P450 cholesterol side chain cleavage; 3β-HSD, 3β-hydroxysteroid dehydrogenase; 17β-HSD1, 17β-hydroxysteroid dehydrogenase 1; P450arom, cytochrome P450 aromatase.

Medicine approved the protocol (permit number: 14016). All animal experimental procedures were performed in accordance with the Guidelines for the Care and Use of Laboratory Animals of the Chinese Animal Welfare Committee.

Wistar rats obtained and raised in this study were housed and mated as preciously described (Xu et al., 2013). A sperm-positive vaginal smear was the confirmation for mating, and this day was considered as gestational day (GD) 0. The pregnant rats were randomly divided into a control group and a PNE group. The PNE group was injected subcutaneously with nicotine (2.0 mg/kg.d), and the control group was given an equal volume of saline from GD9 to GD20. On GD20, some of the pregnant rats were anesthetized by isoflurane inhalation. Pregnant rats with litter sizes of 12–14 offspring (the male/female ratio was approximately 1:1) were selected for the final study, and one female fetus was randomly selected from each litter (n = 12 per group). The fetal blood was collected and centrifuged for serum. Five fetal rats were randomly selected and their ovaries were fixed in freshly prepared Bouin's solution. After 24 h, the ovaries were dehydrated with alcohol and embedded in paraffin for morphological analysis. The remaining fetal ovaries were quickly frozen in liquid nitrogen and stored at 80 °C for further experimental analysis.

The remaining pregnant rats were allowed to normally deliver F1 generation offspring. The number of pregnant rats in each group was set to 8 (the litter sizes were 12–14 at birth, and the male/female ratio was approximately 1:1). After weaning, the female offspring were kept in separate cages. At postnatal week (PW) 12, the F1 females were euthanized with inhaled isoflurane for blood and ovaries.

2.3. Hematoxylin-eosin staining, immunohistochemistry, and transmission electron microscope examination for ovaries

The 5-μm thickness paraffin histological sections were prepared and routinely stained with hematoxylin–eosin (HE). Every 5th section of the series was saved, observed, and photographed with an Olympus AH-2 light microscope (Olympus, Tokyo, Japan). The immunohistochemical (IHC) staining for Ki67, cleaved Caspase-3, and P450arom in the rat ovaries was assessed through the routine IHC streptavidin-peroxidase-conjugated method. Sections approximately 5-μm thick were incubated with antibodies specific to Ki67 (diluted 1:200), cleaved Caspase-3 (1:50), and P450arom (1:100), respectively. Five random fields from each section were examined and analyzed using the Image-Pro Plus 6.0 (Media Cybernetics, Inc. USA).

Fetal ovaries were fixed with 2.5% glutaraldehyde in 0.1 M phosphate buffer (pH = 7.4) for 2 h at 4 °C and post fixed with 1% osmium tetroxide. The samples were dehydrated through a graded series of ethanol and embedded in Epon 812. Ultrathin sections (~50 nm) were cut with the LKB-Vultra microtome (Bromma, Sweden), dually stained with uranyl acetate and lead citrate, and examined with a Hitachi H600 transmission electron microscope (Hitachi, Tokyo, Japan).

To classify follicles and measure the granulosa cell layers' thickness of the antral follicles, five sections from different ovaries with the largest cross-sectional area were used for image analysis. The granulosa cell layers' thickness of the antral follicles was measured in five different sections to evaluate the development of antral follicles.

2.4. Cell culture and treatment

The human granulosa cell line KGN was provided by the Center for Translational Medicine and Jiangsu Key Laboratory of Molecular Medicine (Nanjing, China). The cells were seeded in cell culture flasks (25 cm^2, Corning, USA) that contained Dulbecco modified Eagle medium (DMEM) supplemented with 10% fetal bovine serum (Gibico, USA) and 1% penicillin/streptomycin, cultured in a 5% CO2 humidified incubator at 37 °C. To test the effect of nicotine, the cells were treated with different concentrations of nicotine (0, 0.1, 1, and 10 μM) for 48 h. An MTS assay was conducted to detect the cytotoxicity of nicotine on KGN cells according to the manufacturer's protocol. Absorption intensity was measured at 490 nm using an ELISA reader (TECAN,

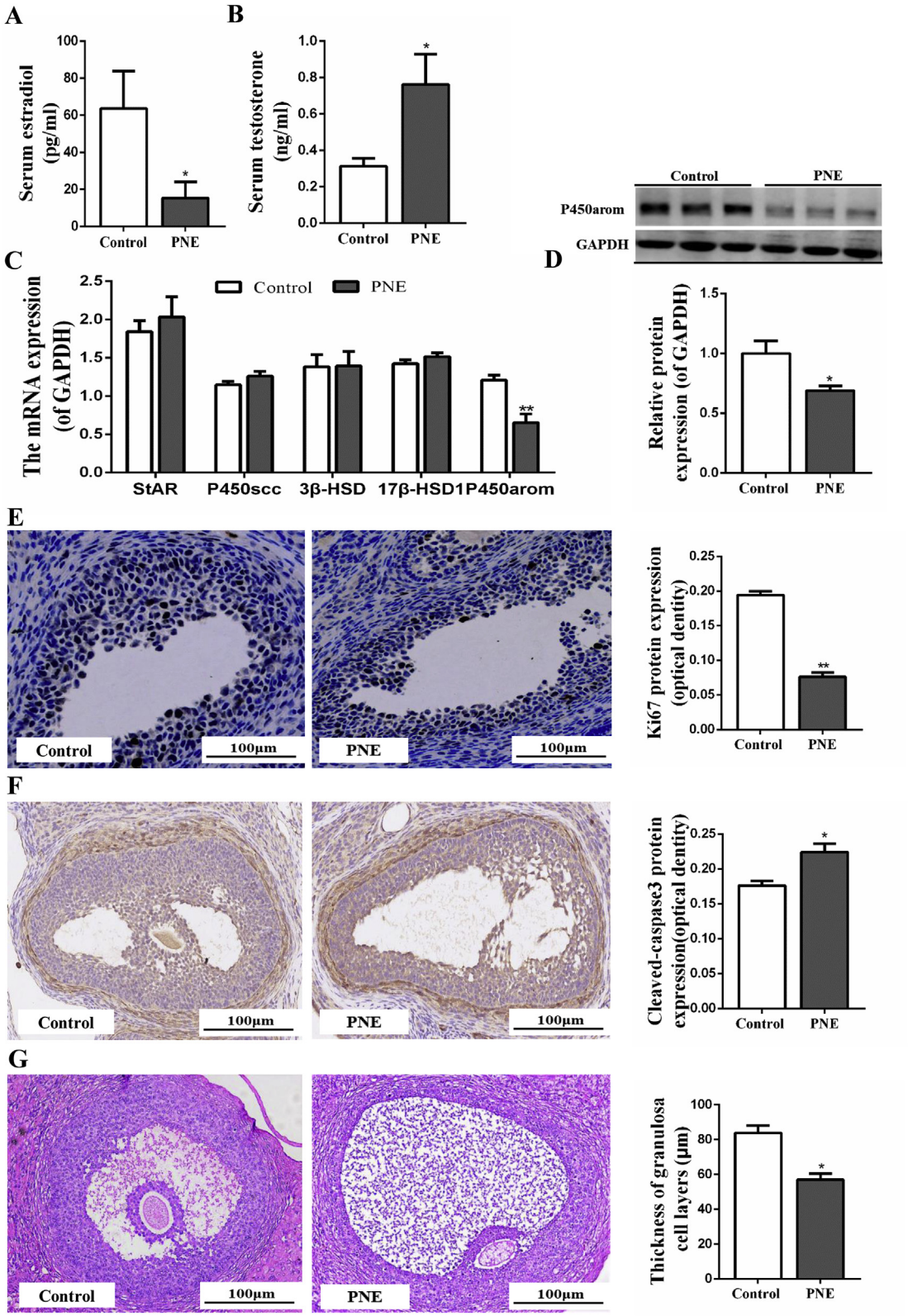

Fig. 3. Effects of prenatal nicotine exposure (PNE) on serum estradiol concentration, ovarian steroidogenic enzymes expression, and antral follicle morphology after birth. A: serum estradiol concentration (n = 8); B: serum testosterone concentration (n = 8); C: the mRNA expression of StAR, P450scc, 3β-HSD, 17β-HSD1 and P450arom (n = 8); D: P450arom protein expression (n = 3); E, F: Ki67 and cleaved caspase-3 protein expression in antral follicle (immunohistochemical, × 200), three sections of each group were selected and five random fields of each section were scored; G: antral follicle morphology (HE, × 200) and the thickness of granulosa cells layers in antral follicle (n = 3). Mean ± S.E.M., $^{*}P < 0.05$, $^{**}P < 0.01$ vs. control.

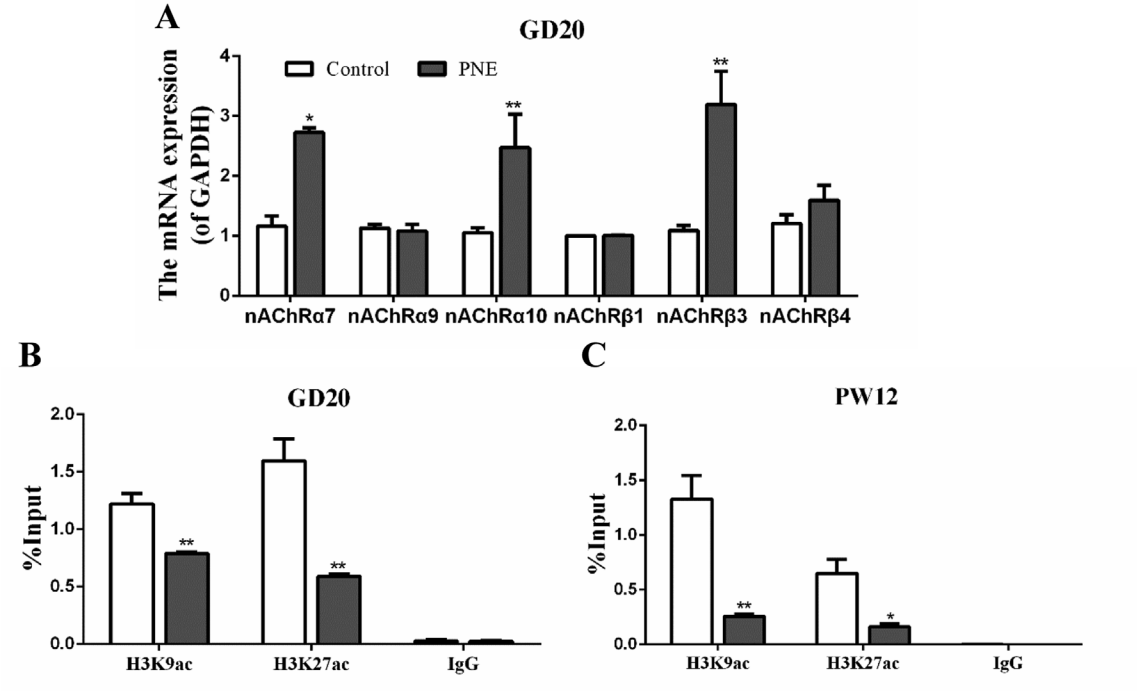

Fig. 4. Effects of prenatal nicotine exposure (PNE) on nicotinic acetylcholine receptors (nAChRs) expression in the fetal ovary and histone acetylation level of P450arom promoter before and after birth. A: the mRNA expression of nAChRs at gestation day (GD) 20 (n = 6, six pairs of fetal ovaries from two littermates were pooled for homogenization into one sample); B, C: chromatin immunoprecipitation (ChIP) assay of P450arom histone acetylation ratio of promoter region in ovary tissue at GD 20 and postnatal week (PW) 12, respectively (n = 3). Mean ± S.E.M., $*P < 0.05$, $**P < 0.01$ vs. control. P450arom, cytochrome P450 aromatase; H3K9ac, histone 3 lysine 9 acetylation; H3K27ac, histone 3 lysine 27 acetylation.

Australia).

To confirm the signaling pathway, nonspecific and competitive nAChR antagonist vecuronium bromide was used. Briefly, the KGN cells were seeded in six-well plates at a 5000 cells/well density; after reaching 30%–50% confluent, the cells were treated with vecuronium bromide (1 μM). After 48 h, the cells were collected for the subsequent analyses.

2.5. Hormone concentration detection for serum

The serum of female fetuses (from 3 to 4 litters) was combined as one sample. The concentration of estradiol in the fetal serum was measured by ELISA assay kit [intra-assay precision: coefficient of variation (CV) < 6.0%; inter-assay precision: CV < 7.1%]. The concentration of testosterone in the fetal serum was measured by ELISA assay kit [intra-assay precision: coefficient of variation (CV) < 2.9%; inter-assay precision: CV < 6.8%]. The RIA kit was used to measure the concentration of estradiol (intra-assay precision: CV < 10%; inter-assay precision: CV < 15%) and testosterone (intra-assay precision: CV < 10%; inter-assay precision: CV < 15%) from postnatal serum samples and the supernatant of KGN cells. All assay procedures followed the manufacturers' protocol.

2.6. Total RNA extraction, reverse transcription, and RT-qPCR for ovaries

The total RNA was extracted from the ovary tissues and KGN cells using the TRIZOL reagent following the manufacturer's protocol. The tissues of littermates were pooled for homogenization as one sample. The concentration and purity of the total RNA were determined using a spectrophotometer (NanoDrop, 2000), and the total RNA concentration was adjusted to 1 mg/mL. Single-strand cDNA was prepared from 1 mg of total RNA according to the manufacturer's protocol and was stored at −20 °C until use. All of the primers were designed using Primer Premier 5.0 (PREMIER Biosoft International, CA). The sequences of each of the designed primers were queried using the NCBI BLAST database for homology comparison and are listed in Table 1. The RT-qPCR was performed using the ABI Step One RT-PCR thermal cycler (ABI Stepone, USA) in a 10-μL reaction mixture. To quantify the gene transcripts more precisely, the mRNA level of the housekeeping gene glyceraldehyde 3-phosphate dehydrogenase (GAPDH) was measured and used as a quantitative control. Each sample was normalized against the GAPDH mRNA level.

2.7. Total protein extract and western blotting assay

Briefly, ovary tissue and KGN cells were rinsed three times with ice-cold phosphate-buffered saline (PBS) and then lysed for 30 min at 4 °C in radioimmunoprecipitation assay (RIPA) lysis buffer containing phosphatase inhibitor cocktail, followed by the BCA Assay Kit for protein quantification. A total of 30 μg of proteins was loaded to each lane, isolated by 10% sodium dodecylsulphate-polyacrylamide gel electrophoresis (SDS-PAGE), and blotted onto polyvinyl diisopropyl fluoride (PVDF) membranes (Millipore, MA, USA). Membranes were blocked in 5% non-fat milk for 1 h and incubated overnight at 4 °C with the primary antibody, including P450arom (1:1000, ab18995) and GAPDH (1:5000, AC002). Then, they were incubated with horseradish peroxidase (HRP)-conjugated secondary antibody for 1 h on an orbital shaker followed by detection with the ECL Plus Western Blotting Detection System (Applied Biosystems). The relative protein level was standardized with GAPDH protein level and compared with controls. The protein bang intensities were analyzed by Image J (National Institutes of Health, Bethesda, Maryland) from three independent bands.

2.8. Chromatin immunoprecipitation-polymerase chain reaction (ChIP) assay

ChIP assay was applied on ovarian tissue of GD20, PW12 of F1

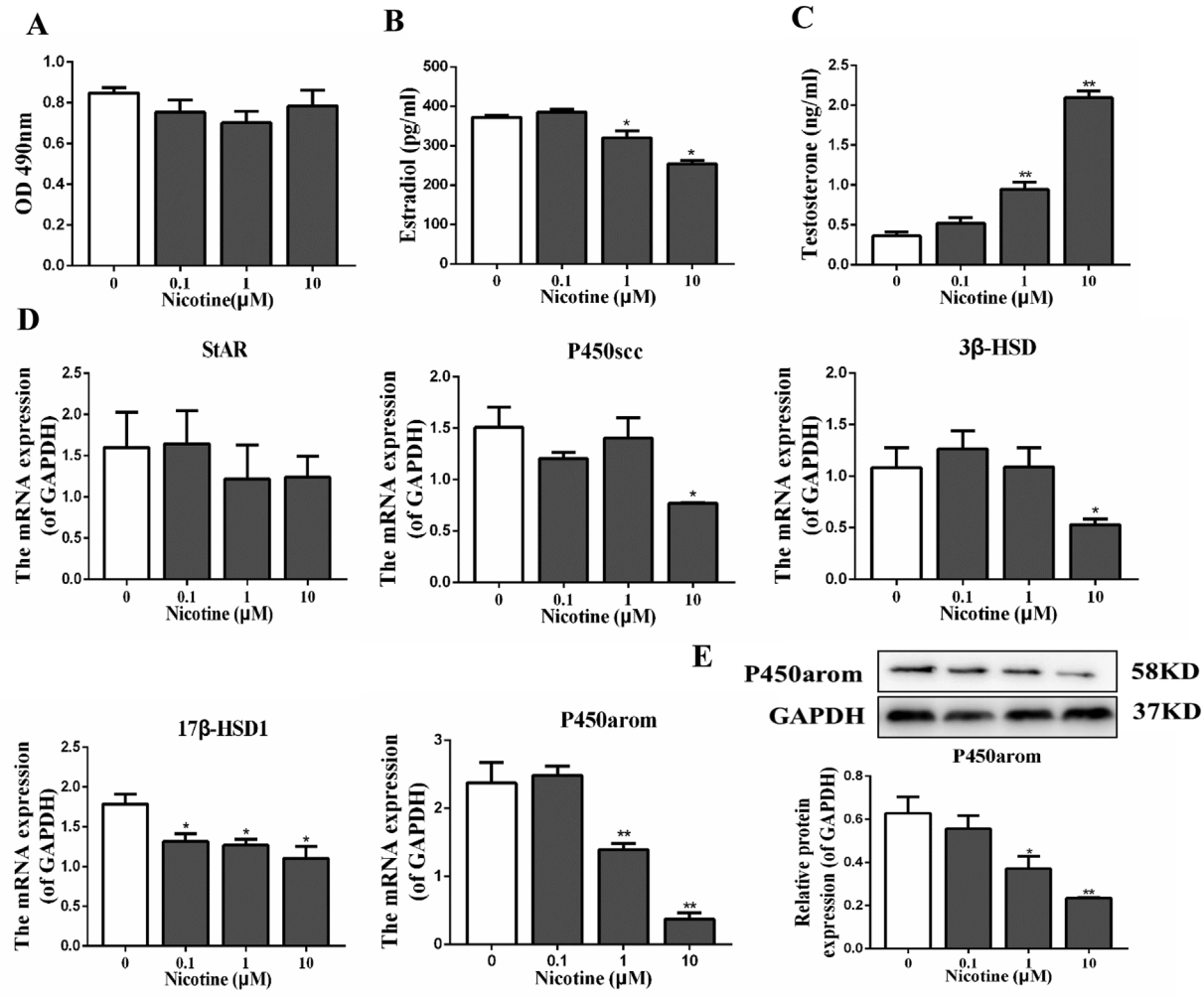

Fig. 5. Effects of nicotine on ovarian estradiol synthesis in human KGN cells. KGN cells were treated with nicotine (0, 0.1, 1, and 10 μM) for 48 h. A: cell viability (n = 6); B: estradiol concentration (n = 6); C: testosterone concentration (n = 6); D: the mRNA expression of StAR, P450scc, 3β-HSD, 17β-HSD1, and P450arom by RT-qPCR (n = 6); E: P450arom protein expression by western blotting (n = 3). Mean ± S.E.M., $^{*}P < 0.05$, $^{**}P < 0.01$ vs. control.

offspring and KGN cells to evaluate H3K9ac and H3K27ac levels at the promoter region of the P450arom gene. The samples were fixed with 1% formaldehyde to cross-link histones to DNA on a rocker at room temperature for 10 min, and the reaction was stopped by adding glycine to the final concentration of 125 mM. After washing by ice-cold PBS, samples (single-cell suspension) were disaggregated by a Dounce homogenizer in lysis buffer supplemented with a protease inhibitor cocktail to aid release of nuclei. The suspension was then centrifuged at 3000 rpm, 4 °C, for 60 s, and the nuclei were resuspended in lysis buffer for sonication to shear DNA to lengths between 200 and 1000 base pairs using SONICS Vibra-CellTM (Cole-Parmer Instruments, Vernon Hills, IL). The sonicated samples of sheared DNA were then incubated with Protein G magnetic beads (Millipore, 16–157) and divided into four parts: the first was used for input DNA; the others were used for immunoprecipitation with anti-acetyl H3K9, anti-acetyl H3K27, and IgG at 4 °C overnight on a rocker. To further obtain DNA fragments for RT-qPCR analysis, the phenol-chloroform method, ethanol precipitation, and resuspension in deionized water were sequentially performed, followed by incubation of proteinase K (200 μg/mL final concentration) the next day at 65 °C. Next, RT-qPCR was conducted as previously described. The sequences of the primers spanning the P450arom binding region used for RT-qPCR are as follows: human: ACCCTCATTCCAGAG GAGGT (forward) and CAGCAAGGTCTGTCTGTCCA (reverse); rat: TGCACGTCACTCTACCCACT (forward) and TGCTGGAATGGACAGAT GTT (reverse). The experiments were conducted in triplicate, and the levels of H3K9ac and H3K27ac at the promoter region were calculated by the fold enrichment method relative to IgG antibody and normalized to the input DNA.

2.9. Statistical analysis

Excel (Microsoft, Redmond, WA, USA) and Prism (GraphPad Software, La Jolla, CA, USA) were used to perform data analysis. Quantitative data were expressed as the mean ± standard error of the mean (S.E.M.). For weights of fetuses, the mean weight of each litter was used for statistical analysis. The Student *t*-test and One-way analysis of variance (ANOVA) followed by a post hoc Dunnett *t*-test or a post hoc Bonferroni *t*-test were performed as appropriate. Statistical significance was designated at $P < 0.05$.

3. Results

3.1. Effects of PNE on ovarian morphology in fetal rats

Firstly, we observed the effects of PNE on the ovarian morphological development in fetal rats. Compared with the control group, the body size of fetuses in the PNE group were smaller (Fig. 1A) and their body weights were significantly lower (Fig. 1B). The maximum mean diameter and the corresponding maximum mean area of the fetal ovaries were both decreased (Fig. 1C/D). At the same time, the expression of

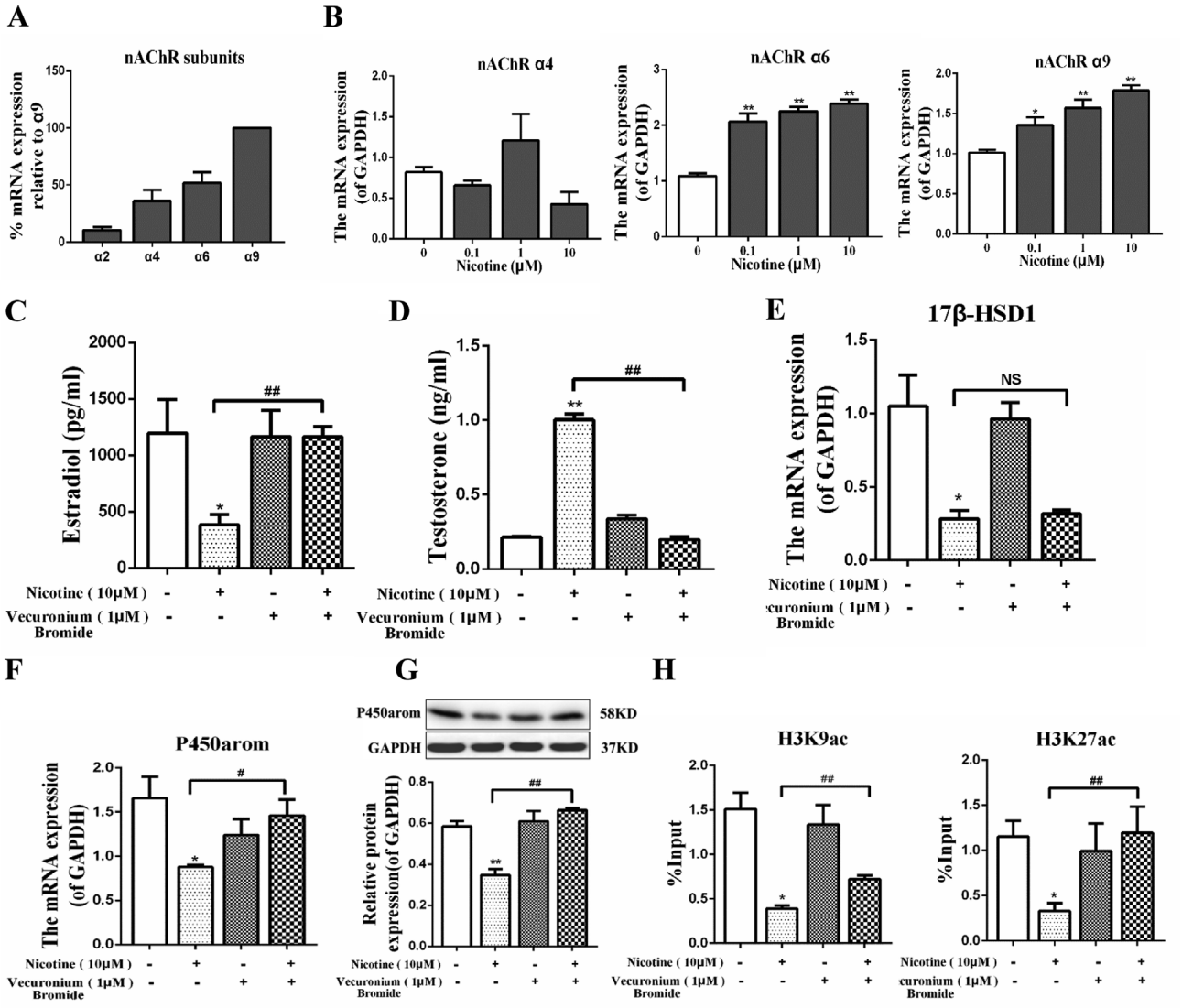

Fig. 6. Effects of nicotine on expression of nicotinic acetylcholine receptors (nAChRs) and the acetylation of histone H3 lysine 9 and 27 (H3K9ac and H3K27ac) of P450arom in human KGN cells. KGN cells were treated for 48 h with 10 μM nicotine, 1 μM vecuronium bromide, or their combination. A: the relative percentage of nAChR subtypes of mRNA expression were determined by comparing to the highest expression of α9 subunit (n = 6); B: the mRNA expression of α4, α6, and α9-nAChR by RT-qPCR (n = 6); C: supernatant estradiol concentration of KGN cells (n = 6); D: supernatant testosterone concentration of KGN cells (n = 6); E: the mRNA expression of 17β-HSD1 was detected by RT-qPCR (n = 6); F: the mRNA expression of P450arom was detected by RT-qPCR (n = 6); G: P450arom protein expression by western blotting (n = 3); H: the H3K9ac and H3K27ac levels in the P450arom promoter region (n = 3). Mean ± S.E.M., $^{*}P < 0.05$, $^{**}P < 0.01$ vs. control. $^{\#}P < 0.05$, $^{\#\#}P < 0.01$ vs. 10 μM nicotine.

Ki67 protein was decreased (Fig. 1E), whereas the expression of cleaved caspase-3 was significantly increased (Fig. 1F). Furthermore, the HE staining of the fetal ovaries showed that the number of oocytes per unit area (10,000 μm^2) was significantly decreased in the PNE group (Fig. 1G). Electron microscopy showed that the mitochondrial ridges in the pregranulosa cells of the PNE group were decreased and vacuolar-like changes occurred (Fig. 1H). These data suggested that PNE could cause abnormal morphological development in the fetal ovary.

3.2. Effects of PNE on ovarian estradiol synthesis in fetal rats

We further observed the effects of PNE on ovarian estradiol synthesis in fetal rats. Compared with the control group, the level of fetal serum estradiol in the PNE group was significantly reduced (Fig. 2A) while the testosterone level was increased (Fig. 2B). The mRNA expression of the steroid synthesizing enzymes, including 3β-HSD, 17β-HSD1 and P450arom, which are involved in the synthesis of estradiol, were also decreased (Fig. 2C). On the other hand, the mRNA expression levels of StAR and P450scc were unchanged. In addition, the IHC showed a consistent decrease in the protein expression of P450arom in the PNE group (Fig. 2D). It suggested that PNE inhibited the estradiol synthesis in fetal rats.

3.3. Effects of PNE on ovarian estradiol synthesis after birth

We continuously tested changes of ovarian steroid synthesis in adult offspring rats at PW12. Compared with their respective controls, serum estradiol level of the PNE group was decreased (Fig. 3A) while the testosterone level was increased (Fig. 3B). The expression of P450arom was significantly reduced (Fig. 3C/D). Moreover, HE staining showed that PNE decreased the thickness of ovarian granulosa cell layers (Fig. 3G), which are involved in estradiol synthesis. At the same time, the expression of Ki67 protein was decreased (Fig. 3E), whereas the expression of cleaved caspase-3 was significantly increased in the antral follicles of the PNE group (Fig. 3F). These results suggested that the inhibited ovarian estradiol synthesis (e.g., low expression of P450arom)

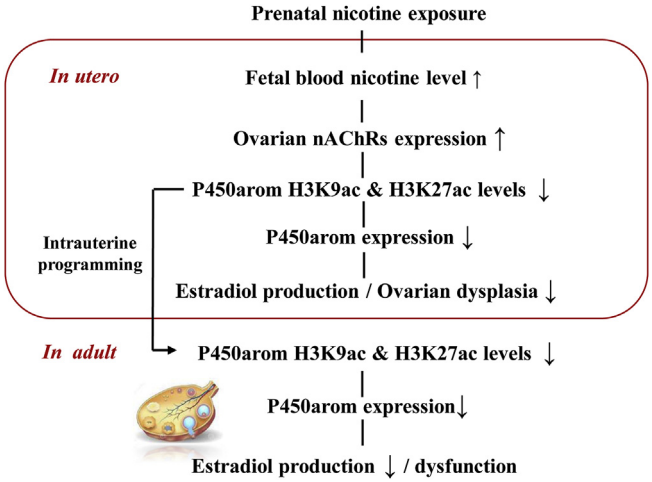

Fig. 7. Intrauterine programming mechanism of ovarian dysplasia and low estradiol synthesis in female offspring rats induced by prenatal nicotine exposure. nAChRs, nicotinic acetylcholine receptors; P450arom, cytochrome P450 aromatase; H3K9ac, histone 3 lysine 9 acetylation; H3K27ac, histone 3 lysine 27 acetylation.

in fetal rats induced by PNE could be sustained to postnatal.

3.4. Effects of PNE on nAChRs expression and histone acetylation of P450arom before and after birth

Given that nicotine plays its role by binding to nicotinic acetylcholine receptors (nAChRs), we also analyzed the mRNA expression levels of different nAChR subtypes in the fetal rat ovary by RT-qPCR, and the expression of nAChRα7, α9, α10, β1, β3, and β4 were detected. Meanwhile, the mRNA expression of nAChRα7, α10, and β3 were significantly increased in the PNE group at GD20 (Fig. 4A). To investigate whether the low expression level of P450arom was associated with altered histone acetylation of its promoter region, ChIP analysis was applied. The results showed that the H3K9ac and H3K27ac levels in the ovarian P450arom promoter region of the PNE group were both significantly lower than those of their controls in GD20 and PW12 (Fig. 4B/C). These results indicated that PNE increased the expression of multiple nAChRs subtypes (i.e., nAChRα7, α10, and β3) in the fetal ovary, and decreased the H3K9ac and H3K27ac levels in the promoter region of P450arom before and after birth.

3.5. Effects of nicotine on ovarian estradiol synthesis in the KGN cells

We previously found that the concentration of serum nicotine in female rats exposed to nicotine at 2.0 mg/kg.d was 0.307 ± 0.147 μM (Tie et al., 2016). Based on this, we set nicotine concentrations (0.1, 1 and 10 μM) to observe its effects on estradiol synthesis in the KGN cell line. The MTS assay showed no significant changes in cell viability after 48 h of nicotine treatment (Fig. 5A). However, nicotine inhibited the estradiol production (Fig. 5B) and the mRNA expression of 17β-HSD1 and P450arom (Fig. 5D), whereas P450scc and 3β-HSD expression were only reduced under high-concentration nicotine treatment, and StAR expression did not change at any concentration (Fig. 5D). The testosterone level was increased (Fig. 5C). Further detection of protein level showed that P450arom expression was significantly reduced by 1 and 10 μM nicotine treatment (Fig. 5E). These results suggested that nicotine could inhibit the estradiol synthesis of ovarian granulosa cells.

3.6. Effects of nicotine on nAChRs expression and P450arom histone acetylation in the KGN cells

We analyzed the expression of nAChRs in the KGN cells by comparing the Ct values between all four studied subtypes at the mRNA level. The most abundant expression was observed for nAChR α9, followed by nAChR α4 and α6, with the least expression observed for nAChR α2 (Fig. 6A). We further detected the higher mRNA expression of nAChR α4, α6 and α9 in the KGN cells after nicotine treatment, and observed that the expression of nAChR α6 and α9 were increased at all concentrations (Fig. 6B). To confirm whether nAChRs subtypes were involved in the inhibitory effects of nicotine on estradiol synthesis, we used vecuronium bromide, a nonspecific and competitive nAChR antagonist, to treat the KGN cells. The results showed that the estradiol level was significantly increased (Fig. 6C) while the testosterone level was decreased (Fig. 6D), and the P450arom expression was increased in both mRNA and protein levels (Fig. 6F/G) after treatment with vecuronium bromide. However, 17β-HSD1 expression had no significant change (Fig. 6E). It suggested that nAChRs were involved in the inhibition of P450arom expression and estradiol synthesis induced by nicotine.

Furthermore, we explored the mechanism of nicotine-mediated continuous low expression of P450arom. The ChIP analysis showed that H3K9ac and H3K27ac levels of the P450arom promoter region were decreased under nicotine administration (Fig. 6H); after vecuronium bromide treatment, the levels of H3K9ac and H3K27ac in the P450arom promoter region were significantly increased (Fig. 6H). In summary, nicotine reduced the H3K9ac and H3K27ac levels at the P450arom promoter region mediated by nAChRs.

4. Discussion

4.1. The ovarian estradiol synthetic inhibition in female offspring rats induced by PNE has intrauterine origin

Active smoking in pregnant women is a major way of fetal exposure to nicotine. Other ways include pregnant women exposed to environmental cigarette smoke, use of smokeless tobacco products (e.g., chewing tobacco), and nicotine replacement therapy (Öberg and Prüss-Üstün, 2010). Previous studies showed that a cigarette contains approximately 1.48 mg of nicotine. According to conversion of body surface area coefficient (1:6.17) between humans and rats (Reagan-Shaw et al., 2008), the exposure dose of nicotine (2.0 mg/kg.d) in the present study is equivalent to 15.3 cigarettes per day for a pregnant woman weighing approximately 70 kg (Zhang et al., 2018). It has been reported that heavy smokers consume as many as 25 cigarettes a day during pregnancy (Bao et al., 2016). Thus, the dose we choose can be reached in real life.

The development during the embryonic period would affect ovarian function in adulthood (Zheng et al., 2014). For example, ovaries of adult rats exposed to nicotine in utero had an increased percentage of apoptotic ovarian cells, abnormal ovarian angiogenesis (Petrik et al., 2009) and impaired fertility (Holloway et al., 2006). In the present study, we also observed changed phenotype of estradiol production in female adult rats, accompanied by the thinner thickness of ovarian granulosa cell layers. However, what has PNE done with early ovarian development? To investigate the intrauterine mechanisms of this change, we used the PNE rat model as previously described (Xu et al., 2013). In utero, we found that PNE could inhibit cell proliferation, promote cell apoptosis and decrease the number of oocytes in the fetal ovary. Meanwhile, the level of fetal serum estradiol decreased in the PNE group. These results suggested that PNE-induced ovarian estradiol synthetic inhibition in adult female offspring has an intrauterine developmental origin.

4.2. Nicotine-induced low P450arom expression via nAChRs may contribute to ovarian estradiol synthetic inhibition

It is known that P450arom plays an important role in the final rate-limiting step of estradiol synthesis (Conley and Hinshelwood, 2001).

The gene that codes for P450arom has been included as major determinant of risk for reproductive system diseases, such as PCOS. The low P450arom expression led to increased androgen level and decreased estrogen level, which affected the development and maturation of follicles, as well as the disordered ovulation (Wang et al., 2017). A study has shown that nicotine treatment reduced P450arom expression in human granulosa cell (Barbieri et al., 1986). In the present study, we observed a continuous decrease in serum estradiol level and ovarian P450arom expression in the PNE group, accompanied by an increase in serum testosterone level. In vitro, nicotine treatment concentration-dependently inhibited P450arom expression and estradiol production, whereas upregulated the testosterone production. A study found that granulosa cells from medium-sized follicles of women with PCOS had little aromatase activity (Erickson et al., 1979). In steroid-induced PCOS female rats, the mRNA expression of P450arom was significantly lower (Aghaie et al., 2018). Although our results didn't show the typical morphological changes of PCOS, the imbalance of estrogen and androgen production induced by low P450arom might have a negative effect on the development of this disease and result in a vicious circle (Escobar-Morreale, 2018). All these findings suggested that the low expression of P450arom induced by nicotine might be involved in estradiol synthetic inhibition, which may further lead to the reproductive system diseases after birth.

Studies have shown that nicotine could inhibit ovarian steroidogenesis, such as significant inhibitory effects on androgen secretion in bovine follicles (Sanders et al., 2002) and basal progesterone release in human luteal cells (Miceli et al., 2005), which were related to the expression changes of ovarian nAChRs. Therefore, we further detected the expression of multiple nAChR subtypes in fetal rat ovary. Among them, the expression levels of nAChR α7, α10 and β3 were increased in the PNE group. Petrik et al. (2009) found that nicotine treatment could result in a high expression of nAChRα7 in rat primary granulosa cells, which was in accordance with our results. As we known, KGN cells have the physiological characteristics of normal ovarian granulosa cells (Xiang et al., 2016) and relatively high levels of P450arom activity. In the present study, we treated KGN cells with different concentrations of nicotine, and found that the expression of nAChR α6 and α9 were elevated, while the expression of P450arom were reduced. Futhermore, these abnormalities were reversed by vecuronium bromide treatment. As shown above, we concluded that nicotine decreased the P450arom expression via nAChRs, thus inhibited the ovarian estradiol synthesis.

4.3. Decreased H3K9ac/H3K27ac levels of P450arom mediated the persistent estradiol synthetic inhibition

Epigenetic modification refers to the phenomenon that the DNA sequence does not change and the gene expression changes, which plays an important role in intrauterine programming (Dolinoy and Jirtle, 2008; Reik et al., 2001). The development of high-grade eukaryotic cells is dependent on normal epigenetic regulation, whereas epigenetic modifications can be influenced by harmful environmental factors in early life and permanently impact on gene expression (Waterland and Jirtle, 2004). It has now become clear that for embryonic development some histone modification marks at specific and important locations were retained, and these are related to developmental origins of some reproductive diseases (Hammoud et al., 2009; Brykczynska et al., 2010). In the present study, the expression of 3β-HSD, 17β-HSD1 and P450arom were all decreased in the fetal ovary, but only that of P450arom was still suppressed in adult offspring ovary. Hence, epigenetic modifications were measured on P450arom.

Studies have shown that PNE altered the histone 3 acetylation status in the promoter region of key genes, thereby suppressing the chondrogenic differentiation of bone marrow-derived mesenchymal stem cells (Tie et al., 2018). Meanwhile, the level of histone 3 acetylation is reported being important for the regulation of P450arom gene expression (Monga et al., 2011). Thus, we hypothesized that changes in histone 3 acetylation may be involved in the persistent low expression of ovarian P450arom induced by PNE. H3K9ac and H3K27ac are common histone H3 acetylated forms and hallmarks of chromatin transcriptional activity, which are involved in the developmental programming (Liu et al., 2018; Xiao et al., 2018). In the present study, PNE caused a decreased change in the H3K9ac and H3K27ac levels of fetal ovarian P450arom promoter, and this change was still evident in adulthood. After nicotine treatment of the KGN cells in vitro, the levels of H3K9ac and H3K27ac in the P450arom promoter were also reduced. The addition of vecuronium bromide reversed the acetylation levels of these two sites. These results suggested that both H3K9ac and H3K27ac were involved in contemporary programming of P450arom expression by nicotine via nAChRs.

5. Conclusion

This study first proposed that the PNE-induced ovarian dysplasia and estradiol synthesis inhibition in female offspring rats had an intrauterine origin. The undelaying mechanism may be related to the decreased H3K9ac and H3K27ac levels of P450arom caused by nicotine via nAChRs (Fig. 7). This study has important theoretical and practical value for a deep understanding of ovarian dysplasia and further exploration of its early warning biomarker.

Author contributions

HW conceived and designed the experiments. GLF and QZ did experimental work and paper writing. YW, FL and YXC were contributed to materials, experiments and analysis tools. YN, WZ (Wen Zou) and WZ (Wei Zhang) were involved in technical assistance, discussion and consulting. All authors reviewed the manuscript.

Acknowledgments

This work was supported by grants from the National Key Research and Development Program of China (2017YFC1001300), the National Natural Science Foundation of China (Nos. 81430089, 81673524), and Hubei Province Health and Family Planning Scientific Research Project (No. WJ2017C0003).

Transparency document

Transparency document related to this article can be found online at https://doi.org/10.1016/j.fct.2019.03.055.

Disclosure statement

The authors declare that they have no competing interests as defined by Food and Chemical Toxicology or other interests that might be perceived to influence the results and discussion reported in this paper. The authors have nothing to disclose.

References

Aghaie, F., et al., 2018. The effects of exercise on expression of CYP19 and StAR mRNA in steroid-induced polycystic ovaries of female rats. Int. J. Fertil. Steril 11 (4), 298–303.
Bainbridge, S.A., Smith, G.N., 2006. The effect of nicotine on in vitro placental perfusion pressure. Can. J. Physiol. Pharmacol. 84 (8–9), 953–957.
Bao, W., et al., 2016. Parental smoking during pregnancy and the risk of gestational diabetes in the daughter. Int. J. Epidemiol. 45 (1), 160–169.
Barbieri, R.L., McShane, P.M., Ryan, K.J., 1986. Constituents of cigarette smoke inhibit human granulosa cell aromatase. Fertil. Steril. 46 (2), 232–236.
Brykczynska, U., et al., 2010. Repressive and active histone methylation mark distinct promoters in human and mouse spermatozoa. Nat. Struct. Mol. Biol. 17 (6), 679–687.
Chen, M., et al., 2007. Nicotine-induced prenatal overexposure to maternal glucocorticoid and intrauterine growth retardation in rat. Exp. Toxicol. Pathol. 59 (3–4), 245–251.
Conley, A., Hinshelwood, M., 2001. Mammalian aromatases. Reproduction 121 (5), 685–695.
Contal, M., et al., 2005. [Neonatal consequences of maternal smoking during pregnancy].

J. Gynecol. Obstet. Biol. Reprod. 34 (1) 3S215-22.
Dolinoy, D.C., Jirtle, R.L., 2008. Environmental epigenomics in human health and disease. Environ. Mol. Mutagen. 49 (1), 4–8.
Erickson, G.F., et al., 1979. Functional studies of aromatase activity in human granulosa cells from normal and polycystic ovaries. J. Clin. Endocrinol. Metab. 49 (4), 514–519.
Ernst, A., et al., 2012. Maternal smoking during pregnancy and reproductive health of daughters: a follow-up study spanning two decades. Hum. Reprod. 27 (12), 3593–3600.
Escobar-Morreale, H.F., 2018. Polycystic ovary syndrome: definition, aetiology, diagnosis and treatment. Nat. Rev. Endocrinol. 14 (5), 270–284.
Gupta, P., et al., 2013. Serum estradiol as a predictor of success of in vitro fertilisation. BJOG An Int. J. Obstet. Gynaecol. 120 209-209.
Hammoud, S., et al., 2009. Sequence alterations in the YBX2 gene are associated with male factor infertility. Fertil. Steril. 91 (4), 1090–1095.
Higgins, S., 2002. Smoking in pregnancy. Curr. Opin. Obstet. Gynecol. 14 (2), 145–151.
Hogg, K., McNeilly, A.S., Duncan, W.C., 2011. Prenatal androgen exposure leads to alterations in gene and protein expression in the ovine fetal ovary. Endocrinology 152 (5), 2048–2059.
Holloway, A.C., Kellenberger, L.D., Petrik, J.J., 2006. Fetal and neonatal exposure to nicotine disrupts ovarian function and fertility in adult female rats. Endocrine 30 (2), 213–216.
Jaenisch, R., Bird, A., 2003. Epigenetic regulation of gene expression: how the genome integrates intrinsic and environmental signals. Nat. Genet. 33 (Suppl. l), 245–254.
Knapczyk-Stwora, K., et al., 2013. Effect of flutamide on folliculogenesis in the fetal porcine ovary–regulation by Kit ligand/c-Kit and IGF1/IGF1R systems. Anim. Reprod. Sci. 142 (3–4), 160–167.
Lang-Muritano, M., et al., 2018. Early-onset complete ovarian failure and lack of puberty in a woman with mutated estrogen receptor beta (ESR2). J. Clin. Endocrinol. Metab. 103 (10), 3748–3756.
Lim, R., Sobey, C.G., 2011. Maternal nicotine exposure and fetal programming of vascular oxidative stress in adult offspring. Br. J. Pharmacol. 164 (5), 1397–1399.
Liu, Y.D., et al., 2017. Long noncoding RNAs: potential regulators involved in the pathogenesis of polycystic ovary syndrome. Endocrinology 158 (11), 3890–3899.
Liu, M., et al., 2018. Decreased H3K9ac level of StAR mediated testicular dysplasia induced by prenatal dexamethasone exposure in male offspring rats. Toxicology 408, 1–10.
Mahalingam, S., et al., 2017. The effects of in utero bisphenol A exposure on ovarian follicle numbers and steroidogenesis in the F1 and F2 generations of mice. Reprod. Toxicol. 74, 150–157.
Martinez-Arguelles, D.B., Papadopoulos, V., 2010. Epigenetic regulation of the expression of genes involved in steroid hormone biosynthesis and action. Steroids 75 (7), 467–476.
Mehta, A., et al., 2015. HDAC inhibitor prevents LPS mediated inhibition of CYP19A1 expression and 17beta-estradiol production in granulosa cells. Mol. Cell. Endocrinol. 414, 73–81.
Meitzen, J., Meisel, R.L., Mermelstein, P.G., 2018. Sex differences and the effects of estradiol on striatal function. Curr. Opin. Behav. Sci. 23, 42–48.
Miceli, F., et al., 2005. Effects of nicotine on human luteal cells in vitro: a possible role on reproductive outcome for smoking women. Biol. Reprod. 72 (3), 628–632.
Monga, R., et al., 2011. Tissue-specific promoter methylation and histone modification regulate CYP19 gene expression during folliculogenesis and luteinization in buffalo ovary. Gen. Comp. Endocrinol. 173 (1), 205–215.
Munetsuna, E., et al., 2018. Maternal fructose intake disturbs ovarian estradiol synthesis in rats. Life Sci. 202, 117–123.
Öberg, M., Prüss-Üstün, J.M., 2010. A Second-hand smoke: assessing the environmental burden of disease at national and local levels. In: WHO Environmental Burden of Disease Series.
Petrik, J.J., et al., 2009. Effects of rosiglitazone on ovarian function and fertility in animals with reduced fertility following fetal and neonatal exposure to nicotine. Endocrine 36 (2), 281–290.
Reagan-Shaw, S., Nihal, M., Ahmad, N., 2008. Dose translation from animal to human studies revisited. FASEB J. 22 (3), 659–661.
Reik, W., Dean, W., Walter, J., 2001. Epigenetic reprogramming in mammalian development. Science 293 (5532), 1089–1093.
Sanders, S.R., Cuneo, S.P., Turzillo, A.M., 2002. Effects of nicotine and cotinine on bovine theca interna and granulosa cells. Reprod. Toxicol. 16 (6), 795–800.
Tehrani, F.R., et al., 2014. Introducing a rat model of prenatal androgen-induced polycystic ovary syndrome in adulthood. Exp. Physiol. 99 (5), 792–801.
Tie, K., et al., 2016. Prenatal nicotine exposure induces poor articular cartilage quality in female adult offspring fed a high-fat diet and the intrauterine programming mechanisms. Reprod. Toxicol. 60, 11–20.
Tie, K., et al., 2018. Histone hypo-acetylation of Sox9 mediates nicotine-induced weak cartilage repair by suppressing BMSC chondrogenic differentiation. Stem Cell Res. Ther. 9 (1), 98.
Wang, C., Zhou, B., Xia, G., 2017. Mechanisms controlling germline cyst breakdown and primordial follicle formation. Cell. Mol. Life Sci. 74 (14), 2547–2566.
Waterland, R.A., Jirtle, R.L., 2004. Early nutrition, epigenetic changes at transposons and imprinted genes, and enhanced susceptibility to adult chronic diseases. Nutrition 20 (1), 63–68.
Xiang, Y., et al., 2016. miR-483 is down-regulated in polycystic ovarian syndrome and inhibits KGN cell proliferation via targeting insulin-like growth factor 1 (IGF1). Med. Sci. Mon. Int. Med. J. Exp. Clin. Res. 22, 3383–3393.
Xiao, H., et al., 2018. Increased H3K27ac level of ACE mediates the intergenerational effect of low peak bone mass induced by prenatal dexamethasone exposure in male offspring rats. Cell Death Dis. 9 (6), 638.
Xu, D., et al., 2013. Prenatal nicotine exposure enhances the susceptibility to metabolic syndrome in adult offspring rats fed high-fat diet via alteration of HPA axis-associated neuroendocrine metabolic programming. Acta Pharmacol. Sin. 34 (12), 1526–1534.
Yang, Y., et al., 2018. Postischemic application of estrogen ameliorates myocardial damage in an in vivo mouse model. J. Surg. Res. 231, 366–372.
Yildiz, D., 2004. Nicotine, its metabolism and an overview of its biological effects. Toxicon 43 (6), 619–632.
Zhang, G., et al., 2018. Placental mechanism of prenatal nicotine exposure-reduced blood cholesterol levels in female fetal rats. Toxicol. Lett. 296, 31–38.
Zheng, W., et al., 2014. Two classes of ovarian primordial follicles exhibit distinct developmental dynamics and physiological functions. Hum. Mol. Genet. 23 (4), 920–928.